ELECTROMAGNETIC MATCHED-FIELD PROCESSING FOR TARGET HEIGHT FINDING WITH OVER-THE-HORIZON RADAR

Michael Papazoglou and Jeffrey L. Krolik
Department of Electrical and Computer Engineering
Duke University
Durham, NC 27708

ABSTRACT

The refraction of over-the-horizon skywave radar signals by the ionosphere facilitates wide-area surveillance. While current systems measure target ground range, azimuth, and velocity they do not estimate target altitude, which is important for classification purposes. In this paper, a method akin to matched-field processing in underwater acoustics is proposed for target height-finding. The approach exploits the delay-Doppler differences between direct and surface-reflected multipath returns from the target. In particular, the coherent sum of these multipath returns can be matched in the complex delay-Doppler space for a single dwell to estimate target altitude, ground range, and radial velocity. In this paper, a maximum likelihood estimate (MLE) of these target coordinates is developed without requiring knowledge of the target backscatter reflection coefficients. The performance of the MLE is evaluated through simulation for an uncertain quasi-parabolic ionosphere and compared to the Cramer-Rao lower bound (CRLB).

INTRODUCTION

Over-the-horizon (OTH) radar takes advantage of the refractive properties of the ionosphere to detect and locate targets at long ranges. An advantage that OTH radar exhibits over conventional line-of-sight radar is the surveillance range of the OTH radar system is not limited by the horizon and terrain [1]. Many signal processing methods for OTH radar concentrate on determining target ground range, azimuth, and velocity by comparing measured delay times of reflected radar signals to delay times predicted by an ionospheric propagation model [2, 3, 4], but are unable to estimate target altitude. In this paper, target height finding for OTH high frequency (HF) radar is approached as a matched field processing (MFP) problem to extract target ground range, altitude, and radial velocity.

In underwater acoustics, MFP is applied for source range and depth localization by matching sensor outputs to the predictions by full field models which incorporate coherent multipath propagation [5]. MFP has also been applied to low angle line-of-sight radar for height finding in the presence of specular multipath reflections from the ground surface [6]. In this paper, MFP is applied after beamforming in complex delay-Doppler space on a single dwell. The signal model used incorporates the coherent specular multipath reflections from the ground as well as refractive propagation through a vertically varying ionosphere.

The scenario considered includes an uncertain multipath environment in which a target is illuminated by a direct path ray and a single ground reflected ray. For the case of no magnetic field and co-located transmitter and receiver, the complex delay-Doppler surface for this scenario consists of the returns due to the three possible transmit/receive ray combinations.

1. DELAY-DOPPLER PROCESSING IN A MULTIPATH ENVIRONMENT

The multipath scenario considered in this paper is illustrated in figure 1. The transmitted signal is a coherent burst of waveforms denoted by $u(t)$ where a single waveform is represented by $u_p(t)$. The length of each waveform is T and the waveform repetition frequency (WRF) is $f_w = \frac{1}{T}$. There are M waveforms transmitted, so the length of the signal, or coherent integration time (CIT) is $T_c = MT$.

The radar return contains contributions from the direct ray and single surface reflection ray, so for the monostatic case three signal paths are possible. Assume the transmitted signal is reflected off of a target with ground range r, altitude z, and radial velocity v. The "two-way" group delay, phase delay, and Doppler shift for path l are represented by τ_{g_l}, τ_{p_l}, and ω_{d_l}, respectively and are functions of the target parameters $\mathbf{\Theta} = [r \ z \ v]^T$ as well as the environment, which is parameterized by $\mathbf{\Phi}$. In this paper a quasi-parabolic ionosphere model is used so $\mathbf{\Phi}$ consists of the critical frequency, layer height, and layer thickness. Letting $\eta(t)$ represent additive noise, the received signal including multipath for an operating frequency ω_0 is

$$s_r(t) = \sum_{l=1}^{L} \alpha_l u(t - \tau_{g_l}) e^{j(\omega_0 + \omega_{d_l})(t - \tau_{p_l})} + \eta(t) \qquad (1)$$

where α_l includes the unknown target reflection coefficient for the l^{th} multipath return and, for the scenario considered here, the number of paths $L = 3$. Operating at a wavelength λ_0, the Doppler shift is

$$\omega_{d_l} = 2\pi \frac{v_t \left(\cos\theta_{l_i} + \cos\theta_{l_r}\right)}{\lambda_0} \qquad (2)$$

where θ_{l_i} and θ_{l_r} are the incident and reflected ray angles, respectively, along path l.

Delay processing is accomplished by matched-filtering the received signal with the transmitted waveform. The received signal is sampled at intervals of T_s seconds. By assuming that the sidelobes of the waveform ambiguity function $\chi(\tau, \omega)$ from neighboring waveforms are negligible, the

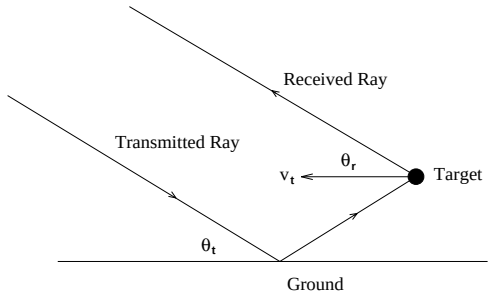

Figure 1. Surface reflection multipath transmission/reflection scenario.

discrete time data representation can be written as

$$x[m,n] \approx \sum_{l=1}^{L} \alpha_l e^{j\psi_l} \chi(nT_s - \tau_{g_l}, \omega_{d_l}) e^{j\omega_{d_l} mT} + \xi_m(nT_s) \tag{3}$$

where n is the sample index within one waveform repetition interval (WRI) and m is the WRI index. Taking a K-point DFT over m yields

$$X[k,n] = \tag{4}$$
$$\sum_{l=1}^{L} \alpha_l e^{j\psi_l} \chi(nT_s - \tau_{g_l}, \omega_{d_l}) P\left(\omega_{d_l} T - \frac{2\pi k}{K}\right) + n_k(nT_s)$$

where

$$P(k) = e^{j\frac{1}{2}k(M-1)} \frac{\sin\left(k\frac{M}{2}\right)}{\sin\left(k\frac{1}{2}\right)} \tag{5}$$

and $n_k(t)$ is the DFT of $\xi_m(t)$ taken across WRI's. Note that in (4) the peaks due to the multipath returns from direct and surface reflected paths are typically unresolved in magnitude but do have a characteristic pattern in complex delay-Doppler space.

To incorporate the delay-Doppler surface into a data vector, the samples from a $M \times N$ subset of the surface $X[k,n]$ are reordered into the $MN \times 1$ vector $\mathbf{x}$ where the model can be written as

$$\mathbf{x} = \mathbf{A}(\mathbf{\Theta}, \mathbf{\Phi})\mathbf{a} + \mathbf{n} \tag{6}$$

where the $(nM+k,l)^{th}$ element of $\mathbf{A}(\mathbf{\Theta}, \mathbf{\Phi})$ is

$$\{\mathbf{A}(\mathbf{\Theta}, \mathbf{\Phi})\}_{nK+k,l} = \chi(nT_s - \tau_{g_l}, \omega_{d_l}) P(\omega_{d_l} T - \frac{2\pi k}{K}), \tag{7}$$

$\mathbf{a}$ is the $L \times 1$ vector of complex reflection coefficients, and $\mathbf{n}$ is the noise vector. Because $\mathbf{a}$ depends on the physical characteristics of the target, it is assumed to be unknown.

2. MAXIMUM LIKELIHOOD ESTIMATION OF TARGET LOCATION

In this section, the maximum likelihood estimate for target ground range and altitude is derived. The target parameters $\mathbf{\Theta}$ and the reflection coefficients $\mathbf{a}$ are considered as non-random unknowns. The environment $\mathbf{\Phi}$ is random with a distribution determined from soundings and historical measurements.

The Maximum Likelihood estimate (MLE) of the target location is determined by maximizing the joint likelihood function of $\mathbf{\Theta}$, $\mathbf{\Phi}$, and $\mathbf{a}$. Assuming the noise is Gaussian distributed with zero mean and covariance $\mathbf{Q}$, and the environment parameters are also Gaussian distributed with mean $\mathbf{m}_\phi$ and covariance $\mathbf{C}_\phi$, the log-likelihood function can be written as

$$L(\mathbf{\Theta}, \mathbf{\Phi}, \mathbf{a}, \mathbf{x}) = L_0 + L_x + L_\phi \tag{8}$$

where

$$\begin{aligned} L_x &= -(\mathbf{x}-\mathbf{s})^H \mathbf{Q}^{-1} (\mathbf{x}-\mathbf{s}) \\ L_\phi &= -(\mathbf{\Phi}-\mathbf{m}_\phi)^H \mathbf{C}_\phi^{-1} (\mathbf{\Phi}-\mathbf{m}_\phi) \end{aligned}$$

and $L_0 = -\log\left[\pi^N (2\pi)^{\frac{M}{2}} |\mathbf{Q}||\mathbf{C}_\phi|^{\frac{1}{2}}\right]$ is a constant term. Note that the term L_x is a function of the match between the model and the observation while L_ϕ is a measure of the *a priori* information of the environment. An estimate of the target parameters is made by maximizing the log-likelihood function

$$\hat{\mathbf{\Theta}}_{ML} = \arg\max_{\mathbf{\Theta}} \left\{ \max_{\mathbf{\Phi}} \max_{\mathbf{a}} [L(\mathbf{\Theta}, \mathbf{\Phi}, \mathbf{a}, \mathbf{x})] \right\} \tag{9}$$

which, by using the model in (6) gives the result

$$\hat{\mathbf{\Theta}}_{ML} = \arg\max_{\mathbf{\Theta}} \left\{ \max_{\mathbf{\Phi}} \left[-\left(\mathbf{P}_A^\perp \mathbf{x}\right)^H \mathbf{Q}^{-1} \left(\mathbf{P}_A^\perp \mathbf{x}\right) - L_\phi \right] \right\} \tag{10}$$

where $\mathbf{P}_A^\perp = \mathbf{I} - \mathbf{A}\left(\mathbf{A}^H \mathbf{Q}^{-1} \mathbf{A}\right)^{-1} \mathbf{A}^H \mathbf{Q}^{-1}$. For cases where a complex electromagnetic propagation model is considered, the maximization over $\mathbf{\Theta}$ and $\mathbf{\Phi}$ in (10) can be implemented numerically. An alternative to maximizing (10) is to maximize the marginal density function by integrating the joint distribution over the random parameters, $\mathbf{\Phi}$. Since the log-likelihood function in (8) is smooth, however a more computationally efficient gradient based optimization algorithm can be used to perform the maximization of (10) whereas integration techniques for the marginal density calculation are typically computationally intensive.

In this paper (10) is maximized by employing the Newton method of descent which entails calculation of the gradient and Hessian matrix of the multidimensional likelihood function. For maximization of a smooth and unimodal function, as is the case here, the Newton method provides rapid convergence.

3. CRAMER-RAO LOWER BOUND

In this section, the Cramer-Rao Lower Bound (CRLB) for the electromagnetic matched field processing application described in this paper is briefly summarized. For a more complete treatment of the CRLB, the reader is referred to [7] and [8].

For this paper, the 12×1 unknown parameter vector is $\mathbf{\Psi}^T = [r_t \; z_t \; v_t \; \mathrm{Re}\{\mathbf{a}\}^T \; \mathrm{Im}\{\mathbf{a}\}^T \; \mathbf{\Phi}^T]$. When there is no *a priori* information on the parameters, the elements of the 12×12 Fisher information matrix (FIM) $\mathbf{J}$ are

$$\{\mathbf{J}\}_{ij} = E\left[-\frac{\partial^2}{\partial\psi_i \partial\psi_j} \ln f_{\mathbf{\Theta},\mathbf{a}}(\mathbf{x}|\mathbf{\Phi}) \right] \tag{11}$$

where the expectation is taken over $\mathbf{x}$. Using the model from (6), the elements of the FIM are

$$\{\mathbf{J}\}_{ij} = 2 \; \mathrm{Re}\left[\frac{\partial \mathbf{s}^H(\mathbf{\Psi})}{\partial\psi_i} \mathbf{Q}^{-1} \frac{\partial \mathbf{s}(\mathbf{\Psi})}{\partial\psi_j} \right] . \tag{12}$$

From (6), $\mathbf{J}$ can be partitioned into

$$\mathbf{J} = \begin{bmatrix} \mathbf{J}_{\alpha\alpha} & \mathbf{J}_{\alpha\phi} \\ \mathbf{J}_{\phi\alpha} & \mathbf{J}_{\phi\phi} \end{bmatrix} \tag{13}$$

where $\mathbf{J}_{\alpha\alpha} =$

$$2\ \mathrm{Re}\begin{bmatrix} \frac{\partial \mathbf{s}^H}{\partial \mathbf{\Theta}}\mathbf{Q}^{-1}\frac{\partial \mathbf{s}}{\partial \mathbf{\Theta}} & \frac{\partial \mathbf{s}^H}{\partial \mathbf{\Theta}}\mathbf{Q}^{-1}\mathbf{A} & \jmath\frac{\partial \mathbf{s}^H}{\partial \mathbf{\Theta}}\mathbf{Q}^{-1}\mathbf{A} \\ \mathbf{A}^H\mathbf{Q}^{-1}\frac{\partial \mathbf{s}}{\partial \mathbf{\Theta}} & \mathbf{A}^H\mathbf{Q}^{-1}\mathbf{A} & \jmath\mathbf{A}^H\mathbf{Q}^{-1}\mathbf{A} \\ -\jmath\mathbf{A}^H\mathbf{Q}^{-1}\frac{\partial \mathbf{s}}{\partial \mathbf{\Theta}} & -\jmath\mathbf{A}^H\mathbf{Q}^{-1}\mathbf{A} & \jmath\mathbf{A}^H\mathbf{Q}^{-1}\mathbf{A} \end{bmatrix},$$

$\mathbf{J}_{\phi\phi} = 2\ \mathrm{Re}\left[\frac{\partial \mathbf{s}^H}{\partial \mathbf{\Phi}}\mathbf{Q}^{-1}\frac{\partial \mathbf{s}}{\partial \mathbf{\Phi}}\right]$ and $\mathbf{J}_{\phi\alpha} = \mathbf{J}_{\alpha\phi}^H =$ $2\ \mathrm{Re}\left[\frac{\partial \mathbf{s}^H}{\partial \mathbf{\Phi}}\mathbf{Q}^{-1}\frac{\partial \mathbf{s}}{\partial \mathbf{\Theta}} \quad \frac{\partial \mathbf{s}^H}{\partial \mathbf{\Phi}}\mathbf{Q}^{-1}\mathbf{A} \quad \jmath\frac{\partial \mathbf{s}^H}{\partial \mathbf{\Phi}}\mathbf{Q}^{-1}\mathbf{A}\right]$. The 9×9 matrix $\mathbf{J}_{\alpha\alpha}$ is the FIM for the nonrandom parameters when the ionospheric parameters are known.

For the case where the *a priori* distribution of the environment parameters is known, the hybrid CRLB is used as a bound on estimation performance [7]. In this case, the FIM is

$$\mathbf{J} = \mathbf{J}_1 + \mathbf{J}_2 \tag{14}$$

where $\mathbf{J}_1 = E[\mathbf{J}]$ with $\mathbf{J}$ from (11) and the expectation taken over $\mathbf{\Phi}$ as well as $\mathbf{x}$. $\mathbf{J}_2$ includes the *a priori* information,

$$\{\mathbf{J}_2\}_{ij} = E\left[-\frac{\partial^2}{\partial\psi_i\partial\psi_j}\ln f(\mathbf{\Phi})\right]. \tag{15}$$

Assuming the environment parameters are Gaussian distributed with mean $\mathbf{m}_\phi$ and covariance $\mathbf{C}_\phi$, then

$$\mathbf{J}_2 = \begin{bmatrix} \mathbf{0} & \mathbf{0} \\ \mathbf{0} & \mathbf{C}_\phi^{-1} \end{bmatrix} \tag{16}$$

which decreases the CRLB as the variance of ionospheric parameters decreases.

4. NUMERICAL SIMULATIONS

To compare the MLE processor with the CRLB, the bounds are determined by numerically computing the derivatives in (12) with finite differences. The performance for the estimator in (10) is illustrated by performing Monte Carlo simulations as a function of signal-to-noise ratio (SNR) and bandwidth (BW).

A quasi-parabolic (QP) propagation model [9] is combined with the delay-Doppler model by using an eigenray finder to calculate group delay and Doppler shift between a transmitter and target as a function of target ground range and altitude. Environmental uncertainty is introduced by considering the critical frequency, layer height, and layer thickness of the QP model as random variables, so the vector of random parameters is $\mathbf{\Phi} = [f_c\ h_m\ y_m]^T$. The profile statistics, $\mathbf{m}_\phi$ and $\mathbf{C}_\phi$ are estimated from scaled vertical ionogram measurements taken at Wallops Island. The amount of environment variability is controlled by scaling $\mathbf{C}_\phi$ by γ^2 where γ corresponds to the percent of variability.

The radar parameters used in the simulations are chosen for a typical OTH radar. The signal center frequency is 10 MHz, the coherent integration time (CIT) is 20 sec, and the waveform repetition frequency is 60 Hz. The target ground range and altitude are 1200 km and 5 km, respectively and the radial velocity is 100 m/s. The number of waveform samples and pulse samples are $N = M = 8$.

In the simulations considered here, white Gaussian noise is assumed with covariance $\mathbf{Q} = \sigma_n^2\mathbf{I}$. Ground range and altitude estimation results from Monte Carlo simulations over 120 random realizations as a function of SNR are shown in figures 2 and 3 along with the performance predicted by the CRLB for 15 kHz bandwidth and $\gamma = 0.25$. The solid line corresponds to the CRLB from (12) where the environment is known and is equal to the mean environment. The dashed line corresponds to the hybrid CRLB from (14) which assumes an uncertain environment with a known distribution. The dash-dot line corresponds the CRLB averaged over $\mathbf{\Phi}$ if the expectation of $\mathbf{J}_1$ in (12) is only taken over $\mathbf{x}$. This differs from the hybrid CRLB in that, instead of taking the expectation of $\mathbf{J}_1$ over $\mathbf{\Phi}$, the expectation is taken of $(\mathbf{J}_1 + \mathbf{J}_2)^{-1}$. The hybrid CRLB predicts increased performance as SNR increases while the averaged CRLB suggests that the estimation performance is eventually limited by the uncertainty of the environment. The MLE performance is plotted with o's for the case where the environment is known and x's when only the environment statistics are known. These results follow the performance predicted by the averaged CRLB where the ground range estimation performance is limited to 800 m due to the environment uncertainty while the altitude estimation performance is not degraded by the uncertainty for a SNR less than 40 dB. The results indicate that, for a bandwidth of 15 kHz, altitude estimation accuracy at 20 dB SNR is better than 500 m.

Intuitively, the ground range estimate is dependent on the absolute group delays and elevation angles of the radar returns, while the altitude estimate depends on the structure of the complex delay-Doppler return. In other words, the information about altitude is contained in the relative differences between the multipath returns. For the multipath scenario presented in this paper, variability in the ionosphere primarily affects the absolute group delays and elevation angles of the signal returns, but has little effect on the structure of the received signal.

Figures 4 and 5 show the CRLB and simulation results as a function of signal bandwidth at 20 dB SNR and $\gamma = 0.25$. These results also illustrate that ground range estimation is sensitive to environment uncertainty while the uncertainty has little effect on altitude estimation. The results suggest that, by increasing the signal bandwidth to 25 kHz, the altitude estimation accuracy is less than 200 m at 20 dB SNR.

5. CONCLUSIONS

In this paper a maximum likelihood approach to target altitude estimation was presented for an uncertain multipath environment. It was shown that although target ground range estimation is sensitive to environment variability, altitude estimation is inherently robust to uncertainties in the environment due to the insensitivity of the complex delay-Doppler surface structure to environment variability. For a signal bandwidth of 25 kHz and 20 dB SNR, altitude estimation performance is predicted to be better than 200 m. The approach presented here can be extended to include ordinary and extraordinary rays due to a magnetic field and increased multipath due to a bistatic radar configuration. The increased multipath complexity will increase

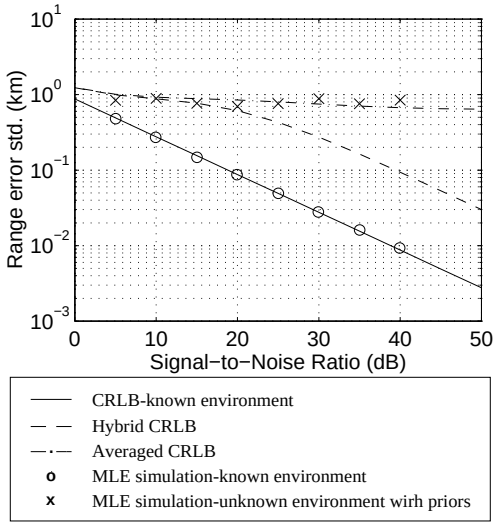

Figure 2. CRLB and MLE simulation results vs. SNR for ground range estimation.

the structure of the complex delay-Doppler surface.

This work was sponsored by ONR under grant number N00014-92-1-1090.

REFERENCES

[1] J. M. Headrick and M. I. Skolnik, "Over-the-horizon radar in the HF band," *Proceeeding of the IEEE*, vol. 62, pp. 664–673, June 1974.

[2] L. F. McNamara, *The Ionosphere: Communications, Surveillance, and Direction Finding*. Krieger Publishing Co., 1991.

[3] L. J. Nickisch and M. Hausman, "CREDO: Coordinate registration enhancement by dynamic optimization," in *Proc. Ionospheric Effects Symposium (IES-96)*, pp. 1B2–1 – 1B2–9, May 1996.

[4] J. L. Krolik and R. H. Anderson, "Maximum likelihood coordinate registration for over-the-horizon radar," *IEEE Transactions on Signal Processing*, 1996. To appear.

[5] A. B. Baggeroer, W. A. Kuperman, and H. Schmidt, "Matched field processing: source localization in correlated noise as an optimum parameter estimation problem," *Journal of the Acoustical Society of America*, vol. 83, pp. 571–587, February 1988.

[6] J. K. Jao, "A matched array beamforming technique for low angle radar tracking in multipath," in *IEEE National Radar Conference*, pp. 171–176, 1994.

[7] Y. Rockah and P. M. Schultheiss, "Array shape calibration using sources in unknown locations – part 1: Far-field sources," *IEEE Transactions on Acoustics, Speech, and Signal Processing*, vol. ASSP-35, pp. 286–299, March 1987.

[8] L. L. Scharf, *Statistical Signal Processing: Detection, Estimation, and Time Series Analysis*. Addison-Wessley Co., 1991.

[9] T. A. Croft and H. Hoogasian, "Exact ray calculations in a quasi-parabolic ionosphere with no magnetic field," *Radio Science*, vol. 3, pp. 69–74, January 1968.

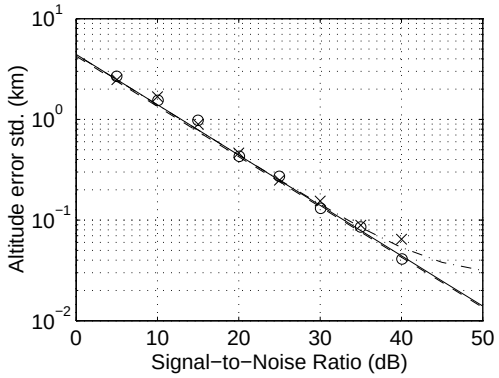

Figure 3. CRLB and MLE simulation results vs. SNR for altitude estimation.

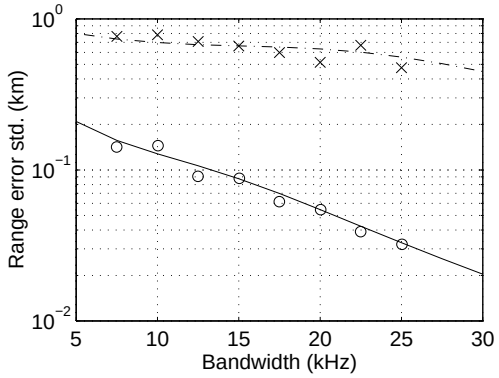

Figure 4. CRLB and MLE simulation results vs. bandwidth for ground range estimation.

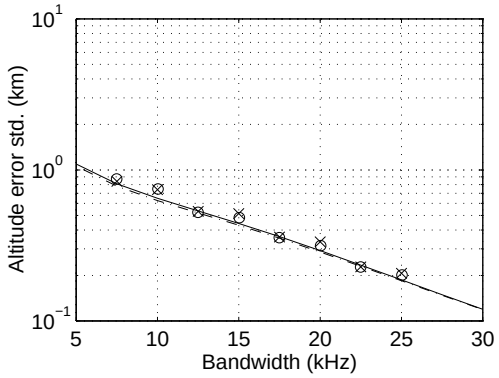

Figure 5. CRLB and MLE simulation results vs. bandwidth for altitude estimation.